Building and Environment 214 (2022) 108845

Contents lists available at ScienceDirect

Building and Environment

journal homepage: www.elsevier.com/locate/buildenv

# Investigation of coupled vapor and heat transport in hygroscopic material during adsorption and desorption

Xiaohai Zhou [a,*], Guylaine Desmarais [b], Stephan Carl [c], David Mannes [d], Dominique Derome [e], Jan Carmeliet [a]

[a] Chair of Building Physics, ETH Zürich, Zürich, Switzerland
[b] Planair SA, Building Physics and Building Retrofit Groups, Geneva, Switzerland
[c] Laboratory of Multiscale Studies in Building Physics, Empa, Dübendorf, Switzerland
[d] Laboratory for Neutron Scattering and Imaging, Paul Scherrer Institute, Villigen, Switzerland
[e] Department of Civil and Building Engineering, Université de Sherbrooke, Sherbrooke, Canada

ARTICLE INFO

*Keywords:*
Wood
Sorption
Latent heat
Moisture buffering
Thermal insulation
Neutron radiography

ABSTRACT

Vapor sorption in hygroscopic porous materials is accompanied by latent heat release/storage, which can influence indoor thermal comfort and building heating and cooling energy consumption. There is a need to better understand the coupled vapor and heat transport during adsorption and desorption. In this study, longitudinal spruce samples are exposed to adsorption and desorption experiments. Neutron radiography provides accurate measurement of moisture content variations spatially and temporally. Wireless thermocouples provide accurate measurements of temperature at different locations. Large changes in moisture content and temperature are observed during both adsorption and desorption experiments. Both moisture content and temperature variations seen in experiments are well simulated with hygrothermal modeling. The latent heat associated with vapor sorption is found to be the source of the large variations in temperature. It is found that vapor permeability influences both vapor and thermal transport while thermal conductivity influences only thermal transport. The vapor transfer coefficient has a small influence on vapor transport while the convective heat transfer coefficient has an influence on heat transport. The validated hygrothermal model is further used to simulate the coupled vapor and heat transport occurring in moisture buffering tests. It is found that moisture buffering values are different by up to 14% depending on the presence or absence of thermal insulation around the samples. For more hygroscopic materials, the difference can be even much larger. It is recommended not only to seal and but also to insulate samples for moisture buffering tests.

## 1. Introduction

It is well known that hygroscopic building materials, like wood, can adsorb significant quantities of moisture. These variations in moisture content display hysteresis between ad- and desorption and are accompanied by changes in temperature due to latent heat and heat of sorption. These coupled heat and sorption processes are ubiquitous in building science and physics. One application, the capability of hygroscopic materials to dampen indoor humidity changes, also referred to as the moisture buffering capacity, has been extensively studied in order to maintain acceptable levels of indoor humidity, thus reducing the risk of moisture-related problems [1–4]. Moisture buffering can indirectly help to reduce ventilation rate contributing to energy savings [5]. Latent heat release/absorption associated with moisture adsorption/desorption in hygroscopic materials can have an influence on indoor thermal comfort and building energy consumption [5–9]. The latent heat associated with moisture sorption can help reduce heating energy consumption in winter and cooling energy consumption in summer.

The temperature distribution in hygroscopic materials can vary significantly as a result of moisture adsorption or desorption. It was reported that desorption cooling from hygroscopic building envelopes could reduce the average operative temperature during heat waves by 1.31° [9]. The energy consumption for heating and cooling in an air-conditioned room can be reduced by 5–30% by using hygroscopic materials [5]. Total energy consumption in buildings can be reduced by up to 25–30% when hygroscopic materials are used in conjunction with

* Corresponding author
*E-mail address:* xizhou@ethz.ch (X. Zhou).

https://doi.org/10.1016/j.buildenv.2022.108845
Received 31 October 2021; Received in revised form 13 January 2022; Accepted 25 January 2022
Available online 31 January 2022

an HVAC system [8]. Temperature increase in an inner solid wood component due to heat of sorption can compensate up to a third of the conductive heat losses through wall elements on a winter day [10].

In most experimental studies on the moisture buffering effect of porous building materials, despite the above-noted concurrent temperature variation, only total moisture change is measured. In some research both moisture and thermal behavior of hygroscopic materials undergoing adsorption and desorption is studied. Charisi et al. [11] studied the hygrothermal behavior of hygroscopic materials under various moisture conditions and found that the main reason for the increase in the surface temperature of porous hygroscopic materials is the amount of vapor adsorbed. Holcroft and Shea [12] compared moisture and temperature changes in different insulation materials during adsorption and desorption and found a correlation between the sorption rate and the heat flux. Zhao et al. [13] studied moisture and temperature changes of wood during adsorption and desorption processes and measured a temperature increase of 2–7 °C and a decrease of 1–6 °C at the very beginning of the adsorption and desorption experiment. James et al. [14] studied moisture and heat transfer in a gypsum bed subjected to a step change in relative humidity and observed mass and temperature increase during adsorption and decrease during desorption. Lelievre et al. studied moisture buffering in hemp concrete samples under slow and fast adsorption/desorption cycling tests and measured different relative humidity changes at the different depths in the sample [15]. The previous studies provide useful insights into the hygrothermal behaviour of porous building materials during adsorption and desorption. However, most of these studies lack high temporal and spatial resolution measurements of moisture and temperature within the materials. In terms of moisture content change measurement, results at the different locations within the samples are not available in the previous studies.

Complementary to experimental work, hygrothermal modeling has been used to study coupled heat and moisture transport in building physics, including aspects related to moisture buffering. Validated and benchmarked commercial codes are available [16,17] and several research models have been developed and validated [18–21]. These coupled moisture and heat models can be used to simulate the hygrothermal behavior of building materials and envelope assemblies [22–24] and evaluate their performance, including freezing and thawing processes in porous building materials [19,25], salt transport [20] and crystallization [26]. These coupled moisture and heat models can be used to study thermal comfort in the indoor environment [9,27] and moisture sorption in porous building materials [15,28,29], and should be considered as investigation tools for further studies on coupled temperature and moisture aspects of sorption.

To this day, two standard experimental procedures have been developed to evaluate the moisture buffering value (MBV) of hygroscopic materials, namely the NORDTEST [30] and the Japanese Test Method [31]. In these two methods, moisture adsorption and desorption are measured on samples that are exposed to cycles between low and high relative humidity during a certain period. The testing samples are sealed on all surfaces but one. The sealing of samples is aimed to introduce a unidirectional vapor transport through the exposed surface. In both test methods, it is assumed that the tests are under isothermal conditions. Although the ambient temperature is constant for the testing samples, moisture adsorption and desorption will lead to temperature increase and decrease in the samples resulting in experiments that are actually under non-isothermal conditions. As a consequence, the materials are exposed to both vapor and heat transport. While vapor transport in MBV tests can be assumed to be unidirectional, heat transport is omnidirectional as the lateral surfaces of the sample are not thermally insulated. Until now, it is not known what is the influence of this non-isothermal heat transport and of thermally insulating the samples on MBV.

In this study, we use advanced measurement techniques to record both temporal and spatial changes of moisture and temperature in a wood sample during adsorption and desorption. The measured moisture and temperature data are then used to validate a hygrothermal model. In a parametric study, the influence of thermal conductivity, vapor permeability and convective heat transfer coefficient on moisture and heat transport is investigated using modeling. Finally, we study the impact of the presence of thermal insulation around a sample on evaluating moisture buffering value.

## 2. Materials and methods

Norway spruce samples, measuring ca. 85.0 mm (radial) x 32.7 mm (longitudinal) x 10.0 mm (tangential), are used for adsorption and desorption experiments (Fig. 1). The wood samples are cut from a piece of Norway spruce extensively characterized by Zillig (2009). The dry bulk density of the samples is 318.1 kg/m$^3$. The samples are preconditioned, then positioned in the test setup and exposed to consecutive conditioning and measuring periods. As preconditioning, the sample for the adsorption experiment is stored in a desiccating cabinet at very low relative humidity (RH), over silica gel particles. The samples for the desorption experiment are stored in a cabinet above a saturated salt solution ($NH_4H_2PO_4$) for several weeks. As a result of this preconditioning, the equilibrium moisture contents of samples for the adsorption and desorption experiments are 1.90 and 17.5 kg/kg, respectively, a moisture content corresponding to equilibrium with a relative humidity of 5.5% and 90.5% RH, respectively, according to the adsorption curve in Fig. 7a.

The sample is mounted inside a custom-made micro-wind tunnel. The walls of the tunnel are made of extruded polystyrene insulation (XPS) to minimize heat and moisture exchanges laterally. The tunnel is configured so that only the top surface of the sample is exposed to air flow (Fig. 1a). The test consists of two periods: the conditioning period and the experimental period. The conditioning period is used to ensure steady initial moisture and temperature conditions in the samples. The sample is subjected to an air flow at a controlled speed of 1.5 m/s at the center of the outlet of the wind tunnel. The temperature and relative humidity of the air is chosen to be similar to the conditions of the samples achieved at the end of preconditioning. The temperature and relative humidity of the air in the conditioning period are shown in Fig. 2a. The indoor air temperature is around 30.0 °C in the experimental chamber. For both the adsorption and desorption samples, the temperature of the incoming air is set at 30.0 °C in the conditioning period to minimize the influence of the ambient environment. The temperature and relative humidity of the incoming air is controlled as follows: for generating air with high relative humidity, compressed air flows through a box with heated water, which leads to an air flow with a temperature around 30.0 °C and relative humidity of around 90%; for generating air with low relative humidity, the compressed air flows through a container filled with silica gel to have relative humidity of around 0%. Then the wet and dry air goes through a thermally insulated tube heated with steel wire at 30.0 °C. For the adsorption sample, the relative humidity of the incoming air is around 3% RH. For the desorption sample, due to the high air flow rate and high air temperature, relative humidity of 90.5% as used in the initial storage period could not be reached. The relative humidity of the incoming air is 82.5%, which is smaller than the preconditioning relative humidity. As a result, there is a small decrease in moisture content in the desorption sample in the conditioning period. The conditioning period is terminated when the mass and temperatures in the samples reach stable values. In the experimental period, the air flow is also maintained at the speed of 1.5 m/s and temperature of 30.0 °C. For the adsorption sample, the relative humidity of the air is increased abruptly from 3% to around 82.5% (Fig. 2a). For the desorption sample, the relative humidity of the air is decreased abruptly from 82.5% to around 1% (Fig. 2a). During the experiments, the temperature and relative humidity of the experimental room is around 30.0 °C and 37% RH, respectively.

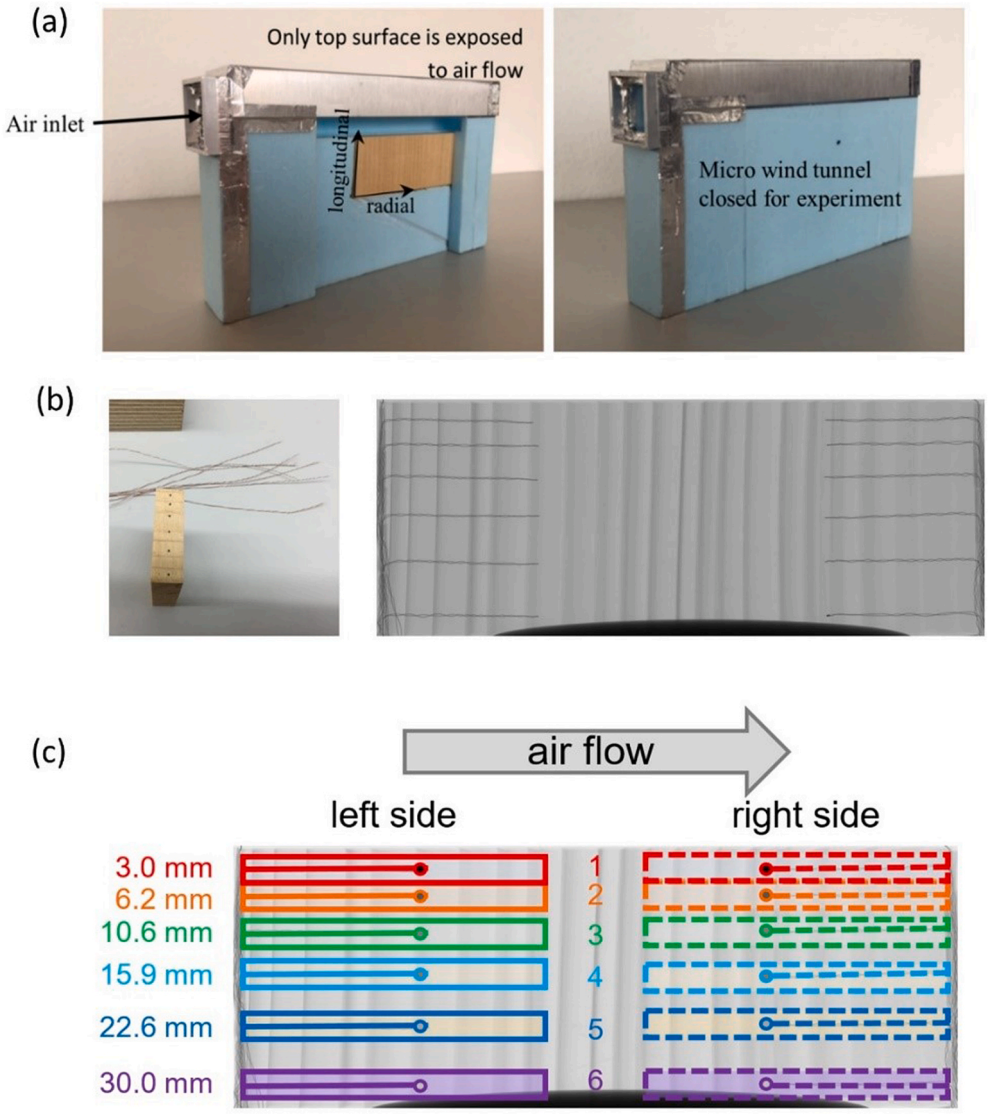


**Fig. 1.** **(a)** Photographs of experimental set showing a sample inside the micro-wind tunnel (left) and the closed setup (right); (b) wood sample showing the holes to insert the thermocouples (left) and X-ray radiography of wood sample showing the locations of thermocouples, showing the longitudinal direction is vertical (right); (c) Positions of thermocouples and corresponding zones for moisture content quantification.

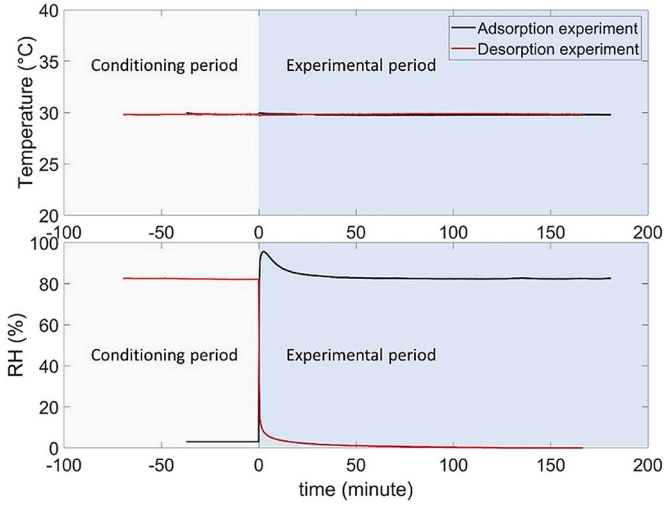


**Fig. 2.** Temperature and relative humidity (RH) of the incoming air during the conditioning and experimental periods for adsorption (black line) and desorption (red line).

### 2.1. Temperature measurement

To monitor temperature, twelve high-gage thermocouples are inserted horizontally from either end of the sample, 20 mm deep, at six different heights, so locating half of the thermocouples on each side (Fig. 1b). The thermocouples are Type T Thermocouple with wire diameter of 0.1 mm. The thermocouples are connected to a Multiplexer. An AnalogDigital-Converter is used to convert analog data to digital data. An Arduino Micro Development Board is used to collect data. A wireless transmitter is used to transmit data to a receiver connected to a computer. This entire wireless measurement system is powered by a 5-V power bank. The wireless transmission rate is 250 Kbps. The resolution of temperature measurement is mainly affected by the voltage measurement, which is around 0.01 °C. The accuracy of temperature measurement is around 0.15 °C. For the full duration of the experiment, temperature data is acquired every 20 s through the wireless transmitter. This wireless temperature measurement system is selected to avoid the interference of wires allowing to weigh accurately the total mass throughout the experiment.

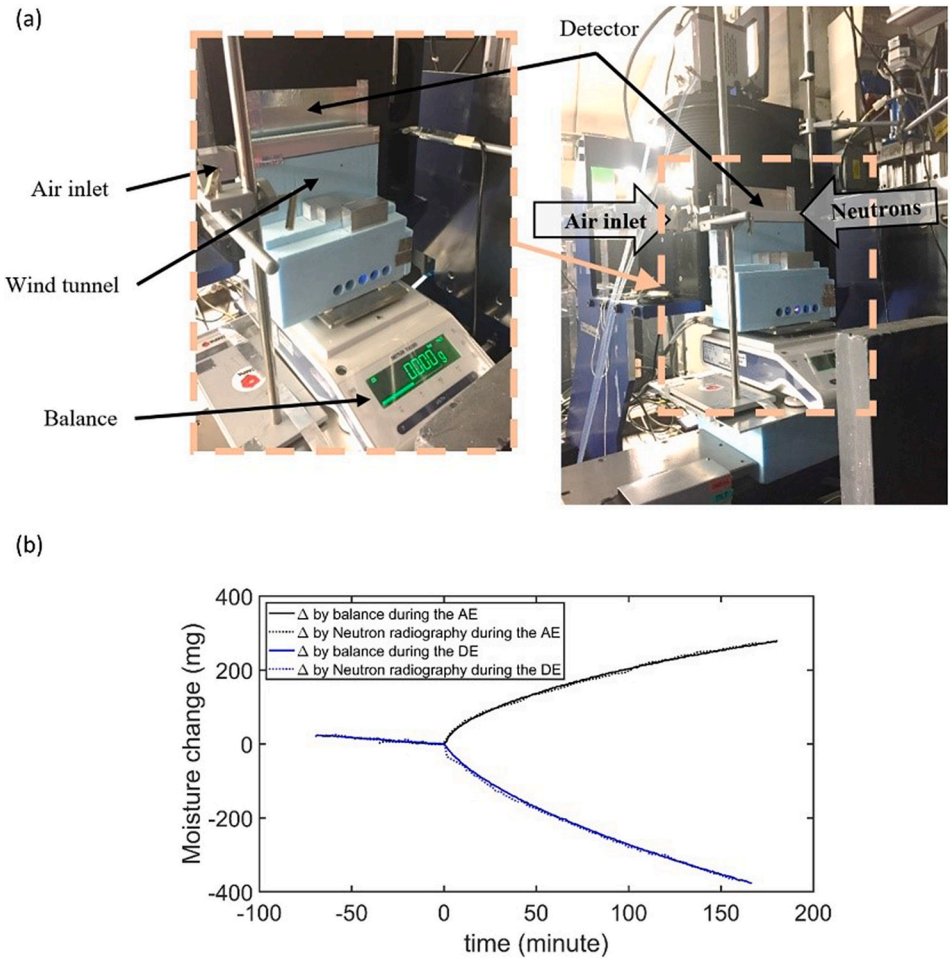


**Fig. 3.** (a) Overall view of the experimental setup in the ICON beamline at PSI, with inset view of the wind tunnel resting on the mass balance; (b) Moisture change Δ in the adsorption (AE) and desorption (DE) experiments.

### 2.2. Moisture content measurements

#### 2.2.1. Moisture content by gravimetry

The average moisture content is acquired by gravimetric measurement. The samples are weighed just before being inserted into the micro-wind tunnel and also at the end of the experiment. In addition, the micro-wind tunnel as a whole, i.e. with sample inserted, thermocouples and wireless transmitter, is placed on a high precision balance (of 0.1 mg accuracy) (Fig. 3). The mass is acquired every 20 s for the whole duration of the experiment. These gravimetric measurements allow us to determine the average moisture content over time. The mass is also used to verify the moisture content determined by neutron radiography.

#### 2.2.2. Moisture content by neutron radiography

Neutron radiography is a powerful non-destructive technique that has been used to measure the time- and space-resolved moisture content distribution in porous building materials [32–34]. Neutron radiography quantification is based on the intensity measurement of a neutron beam transmitted through an object. The intensity of the transmitted monochromatic beam, $I$, can be described with the Beer-Lambert law:

$$I = I_0 e^{-\Sigma . z} \tag{1}$$

where $I_0$ is the intensity of the incident neutron beam (W), $z$ is the thickness of the object along the beam direction (m) and $\Sigma$ is the effective attenuation coefficient for neutrons (1/m). For post-processing, the composition of the tested sample is assumed to consist of two parts: solid material and water. Initially, at time $t_0$, the effect of moisture in the material on the neutron beam attenuation is considered equivalent to the effect of an effective liquid layer with thickness $z_0$ added to the solid sample. Implementing this description, equation (1) becomes:

$$I_{ini} = I_0 e^{-\{\Sigma_s . z_s + \Sigma_l . z_0\}} \tag{2}$$

where the subscript $s$ refers to the solid wood and $l$ to the moisture. At a certain time $t$ during the experiment, the change in the beam intensity is due to the time dependent change of moisture content with respect to the initial stage, i.e. from the thickening or thinning of the "effective" liquid layer $z_l(t)$. Equation (3) describes I(t) as function of $I_{ini}$ as:

$$I(t) = I_{ini} e^{-\{\Sigma_l . z_l(t)\}} \tag{3}$$

Solving for the change in liquid thickness yields:

$$z_l(t) = -\frac{1}{\Sigma_l} ln\left(\frac{I(t)}{I_{ini}}\right) \tag{4}$$

Multiplying the effective liquid layer thickness by its density and dividing by the sample thickness, $z$, yields the moisture content (kg/m$^3$).

$$w(t) = -\frac{\rho_l}{z . \Sigma_l} \ln\left(\frac{I(t)}{I_{ini}}\right) = \frac{\rho_l}{z . \Sigma_l} \left(ln I_{ini} - \ln I(t)\right) \tag{5}$$

In other words, moisture content can be determined by subtracting the natural logarithmic of the image at time t from the natural logarithmic of the initial image of the material.

In this study, the whole setup is placed in the path of a cold neutron beam, the ICON beamline at the Paul Scherrer Institute (PSI) in Villigen, Switzerland (Fig. 3a). Neutron radiography images are taken about

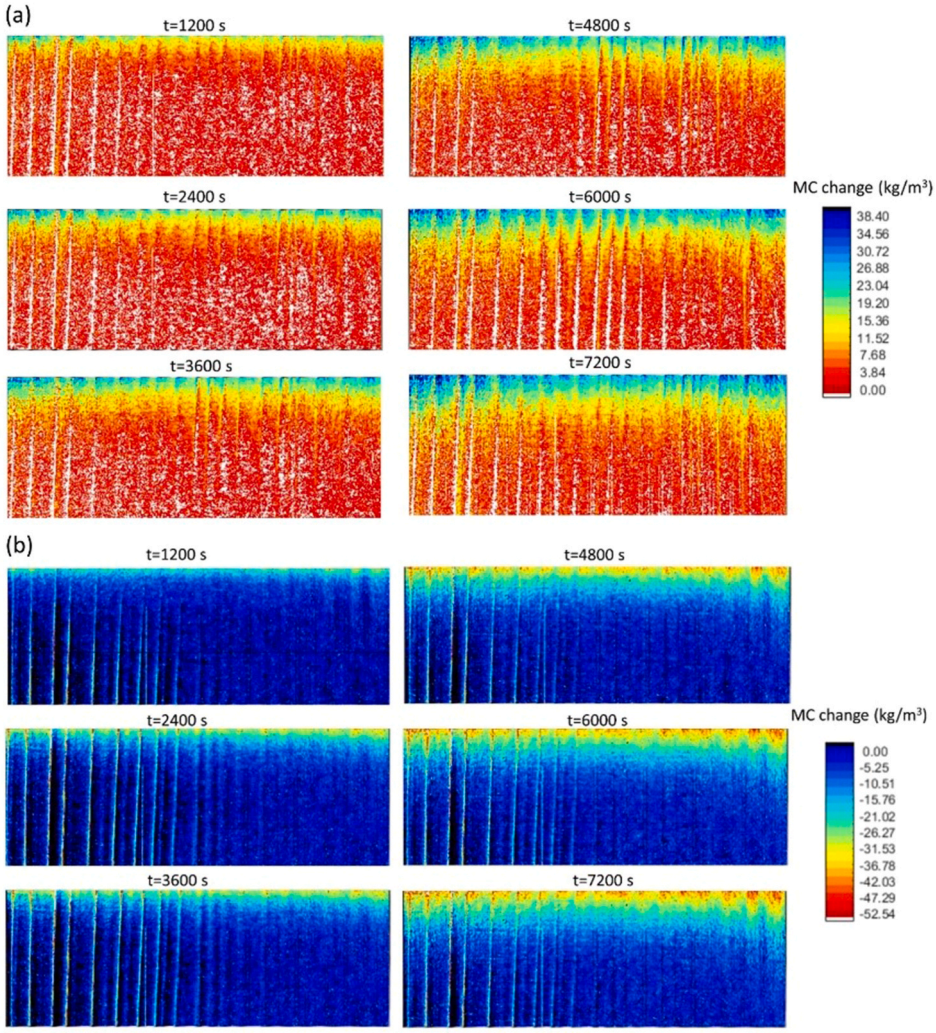


**Fig. 4.** (a) Moisture content (MC) change at six time instances during adsorption experiment; (b) Moisture content (MC) change at six time instances during desorption experiment.

every 8 s with an exposure time of 7 s. The resolution of the images is that of the pixel size, i.e. 45 μm. The Quantitative Neutron Imaging (QNI) algorithm [33], which is based on the iterative reconstruction of the measured image by overlapping point scattered functions calculated using Monte-Carlo simulation, is used to obtain the moisture content change. As wood swells (shrinks) during adsorption (desorption), an affine registration process is applied to the images obtained before post-processing.

## 3. Experimental results

Fig. 3b shows the mass change in the wood samples due to the adsorption and desorption of moisture. The solid lines show the results obtained from the balance, while the dotted lines show the mass variation from neutron radiography analysis for the same experiment. There is excellent agreement between the mass obtained from balance measurement and neutron radiography analysis. For the desorption experiment, there is a small decrease in moisture in the conditioning period. As mentioned above, this decrease is due to lower relative humidity in the incoming air flow than in the pre-conditioned wood sample. The total moisture change in the desorption experiment is larger than in the adsorption experiment.

Fig. 4 shows the two-dimensional distribution of moisture content change in the adsorption and desorption experiments, with Fig. 4a showing the progressive gain in moisture and Fig. 4b the moisture loss at six time instances through the experiment. In general, moisture content closer to the top surface shows a larger change than at a greater depth. For the same depth, there is some difference in moisture content change along the 85 mm width of the sample. This difference reflects material heterogeneity of wood which consists of earlywood and latewood. The difference in earlywood and latewood is shown in Fig. 20 in Zillig (2009). The cells are much larger in earlywood than latewood. Due to the lower density and larger cell cavities of earlywood, vapor permeability is larger in earlywood than in latewood. As a result, vapor transfer and sorption is faster in earlywood than in latewood. Although there is some variation in moisture content change horizontally, the averaged moisture content at the left and right sides of the samples shows very similar variations in Fig. 5a. The material heterogeneity could also be the reason for the small difference in the measured temperatures at the left and right sides in Fig. 5b.

Given the simultaneous measurement of temperature and moisture content in this experiment, moisture content variation results are presented for the zones corresponding to the temperature measurements, assuming the thermocouples (TC) to be centered in a TC zone. Fig. 1c shows the thermocouple and zone locations, overlaid on an actual X-Ray radiography of a wood sample. The dots at the end of the lines indicate the locations of the thermocouples, while the rectangles show the associated TC zones. The depth of the thermocouples from the top

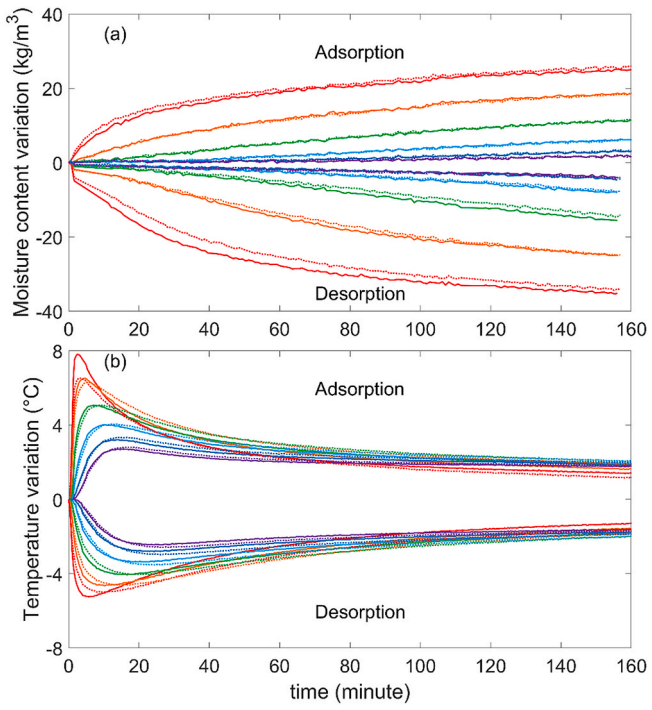


**Fig. 5.** (a) Moisture content variation and (b) temperature variation during adsorption and desorption experiments (solid line represent measured results at the left side; dotted lines represent measured results at the right side, color scheme is explained in Fig. 1c).

surface is indicated in mm on the left side of the sample. In all graphs to follow, the curves go from red at the top to purple for the zones furthest from the top surface (air flow), and are represented by solid lines for the left side and dotted lines for the right side. The area of all the TC zones is 40 mm × 4 mm (i.e. 2 mm above and 2 mm below the thermocouple).

Fig. 5a presents the moisture content variation (moisture content at time $t$ minus initial moisture content) for each TC zone for the adsorption and desorption experiments. There is no significant difference between the left side (solid lines) and the right side (dotted lines) of the sample. During the adsorption experiment, the moisture content variation is almost the same on both sides. By inspection, we note a small difference of moisture content variation at the left and right sides during the desorption experiment at the top two positions. The difference could be due to material heterogeneity and thus different hygrothermal properties between the two sides. The moisture content variation is larger closer to the top surface than at a greater depth. The rate of moisture change is larger at the beginning of the experiments and decreases gradually with time.

Fig. 5b presents the temperature variation for each TC zone for adsorption and desorption experiments. In general, there is no significant difference between the left side (solid lines) and the right side (dotted lines) except in Zone 1 during the adsorption experiment. Zone 1 at the right side during the adsorption experiment shows a smaller temperature increase than that at the left side. Besides, the temperature increase at the right side in Zone 1 is similar to that in Zone 2, while it is expected to be larger than in Zone 2. The smaller increase at the right side in Zone 1 may be due to the inaccuracy of the sensor at this location. During the adsorption and desorption experiment, there is a very large change of temperature at the very beginning of the experiment. Then the temperature change becomes gradually smaller. The temperature change is larger in the adsorption experiment than in the desorption experiment. For example, the largest temperature change is 7.8 °C in Zone 1 during the adsorption experiment while it is only 5.2 °C in Zone 1 during the desorption experiment.

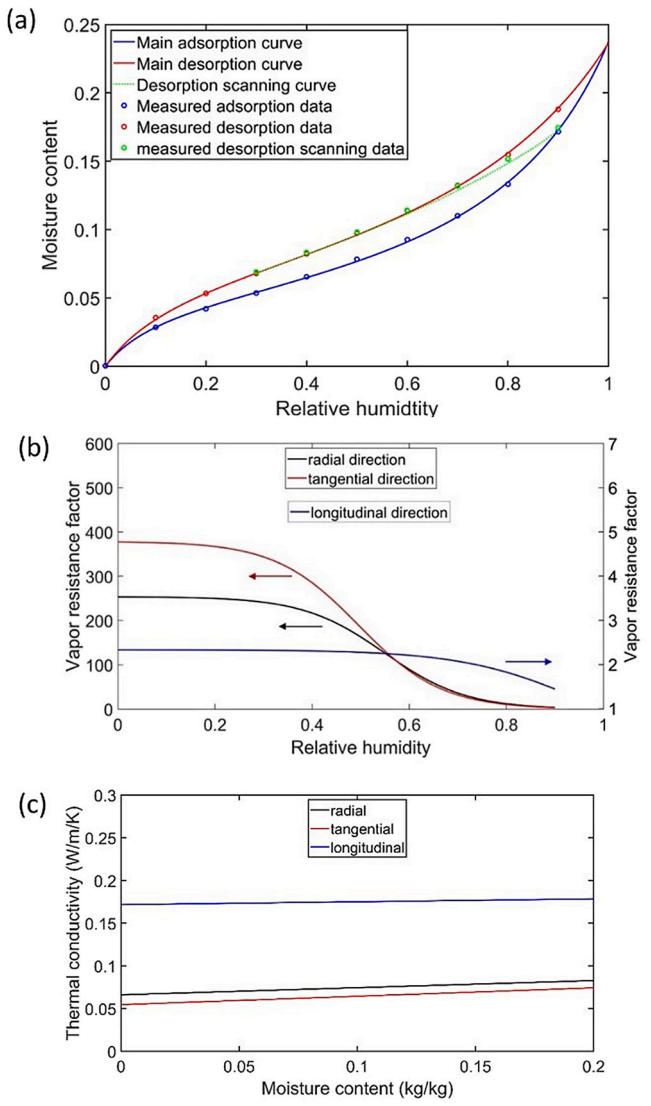


**Fig. 6.** (a) Sorption curves of spruce wood, in dash lines from experimental results and continuous lines from fitted models; (b) Vapor resistance factor in three directions of spruce wood; (c) Thermal conductivity in three directions for spruce wood at the density of our samples.

## 4. Numerical simulation

### 4.1. Governing equations for moisture and heat transport

Even though the heat and moisture transport in the experiments can be considered to be two-dimensional, and eventually unidimensional, we will model our experiments three-dimensionally due to the orthotropic nature of wood, i.e. its material properties in longitudinal, tangential, and radial directions are different. The governing equations for three-dimensional coupled moisture and heat transport in the wood sample are described below, based on [18]. In the current model we only consider vapor transport. Vapor transport in the wood is described with Fick's Law ($g_v = -\delta_v \nabla p_v$). Following [26], we use the capillary pressure as driving potential also for vapor transport. The governing equation of moisture conservation is:

$$\frac{\partial w}{\partial p_c}\frac{\partial p_c}{\partial t} + \frac{\partial}{\partial x_i} g_v = 0 \tag{6}$$

with vapor flow:

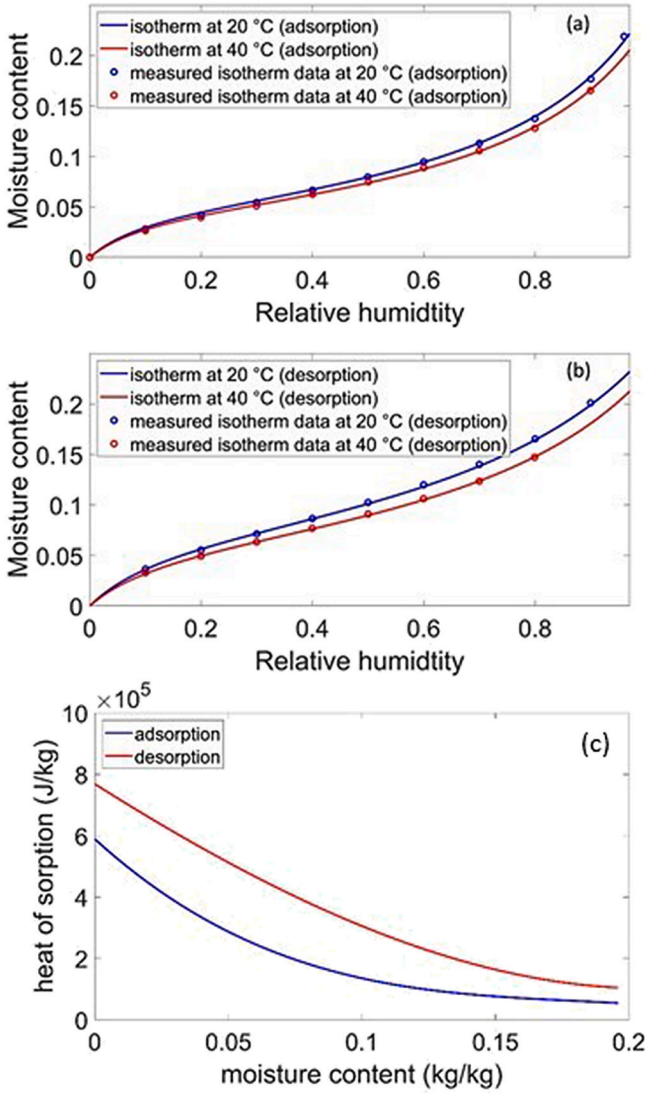


**Fig. 7.** (a) Adsorption isotherms at 20.0 and 40.0 °C; (b) desorption isotherm at 20.0 and 40.0 °C; (c) differential heat of sorption in adsorption and desorption.

$$g_v = -\delta_{i,j}(RH)\cdot\frac{p_v}{\rho_l\cdot R_v\cdot T}\cdot\frac{\partial p_c}{\partial x_j} - \delta_{i,j}(RH)\cdot\frac{p_v}{\rho_l\cdot R_v\cdot T^2}(\rho_l\cdot L_v)\cdot\frac{\partial T}{\partial x_j} \tag{7}$$

The governing equation of energy conservation is:

$$(c_0\cdot\rho_0 + c_l\cdot w)\cdot\frac{\partial T}{\partial t} + \nabla\cdot\left(\left(c_v\cdot\left(T - T_{ref}\right) + L_m\right)\cdot g_v\right) = -\frac{\partial}{\partial x_i}\left(\lambda_{i,j}(w)\frac{\partial T}{\partial x_j}\right) \tag{8}$$

where $w$ is the moisture content (kg/m$^3$), $p_c$ is the capillary pressure (Pa), $g_v$ is the vapor flow flux (kg/m$^2$s), $i, j = 1, 2, 3$ ($x_1 = x$, $x_2 = y$, $x_3 = z$), $\delta_{i,j}(w)$ is the water vapor permeability (s), $p_v$ is the vapor pressure (Pa), $\rho_l$ is the density of water (kg/m$^3$), $R_v$ is the gas constant of water (J/kg K), $T$ is the temperature (K), $c_0$ is the specific heat capacity of spruce (J/kg K), $c_l$ is the specific heat capacity of water (J/kg K), $c_v$ is the specific heat capacity of vapor (J/kg K), $\rho_0$ is the density of spruce (kg/m$^3$), $T_{ref}$ is the reference temperature (273.15 K), $\lambda_{i,j}(w)$ is the thermal conductivity (W/mK), $L_m$ is the latent heat of moisture in wood (J/kg). The latent heat of moisture is defined as:

$$L_m = L_v + \Delta H_s \tag{9}$$

where $L_v$ is the latent heat of vaporization (J/kg) and $\Delta H_s$ is the differential heat of sorption (J/kg).

Assuming that the coordinate axes x, y and z are aligned with the longitudinal, tangential, and radial directions, the vapor flow can be described with the following equation:

$$g_v = -\frac{p_v}{\rho_l\cdot R_v\cdot T}\left(\vec{\delta}(RH)\nabla p_c\right) - \frac{p_v}{\rho_l\cdot R_v\cdot T^2}(\rho_l\cdot L_v)\cdot\left(\vec{\delta}(RH)\nabla T\right) \tag{10}$$

The governing equations (6) and (8) can be reformulated to

$$\frac{\partial w}{\partial p_c}\frac{\partial p_c}{\partial t} - \frac{p_v}{\rho_l\cdot R_v\cdot T}\left(\nabla\cdot\vec{\delta}\nabla p_c\right) - \frac{p_v}{\rho_l\cdot R_v\cdot T^2}(\rho_l\cdot L_v)\left(\nabla\cdot\vec{\delta}\nabla T\right) = 0 \tag{11}$$

$$(c_0\cdot\rho_0 + c_l\cdot w)\cdot\frac{\partial T}{\partial t} + \nabla\cdot\left(\left(c_v\cdot\left(T - T_{ref}\right) + L_m\right)\cdot g_v\right) = -\left(\nabla\cdot\vec{\lambda}(w)\nabla T\right) \tag{12}$$

This heat and moisture model has been validated against HAM-STADT benchmarks [35].

### 4.2. Moisture properties

The adsorption and desorption isotherms are described with the Guggenheim-Anderson-de Boer (GAB) model [36–38]:

$$w = \frac{w_m c k\varphi}{(1 - k\varphi)(1 + k(c-1)\varphi)} \tag{13}$$

where $w$ is the equilibrium moisture content (kg/kg), $\varphi$ is the relative humidity, and $w_m$, $c$, and $k$ are fitting parameters. We assume we can apply with sufficient accuracy this GAB model to wood. The main sorption isotherms are measured with a dynamic vapor sorption device (DVS Endeavour) at different specified relative humidities, with a mass resolution of 1 μg. The sorption isotherms are determined at 30.0 °C. The equilibrium criterion (ration change in mass versus time increment, dm/dt) for the DVS instrument is 0.002%/min for a minimum of 60 min. For the adsorption experiment, the sample follows the main adsorption curve. For the main adsorption curve, the sample is first dried to 0% RH, followed by progressive sampling from 10 to 90% RH in 10% RH increments, followed by sampling at 95% RH. The main desorption curve is measured by reversing the humidity steps. Considering the initial relative humidity of the desorption sample is 90.5%, the desorption experiment follows a desorption scanning curve. Therefore, a desorption scanning curve is measured. First the sample is exposed to adsorption until 90% RH, then followed by sampling from 90% to 30% RH in 10% RH increments. The resulting sorption isotherms are shown in Fig. 6a. The main adsorption curve is used for modelling the adsorption experiment while the desorption scanning curve is used for modelling the desorption experiment.

The vapor resistance factor of spruce wood is described with an exponential function dependent on RH:

$$\mu = \frac{1}{a + b\cdot\exp(c\cdot RH)} \tag{14}$$

where a, b and c are model parameters. Vapor transport is predominately occurring in the longitudinal direction. For the longitudinal direction, the values of a, b and c are first obtained from Zillig [39] and then adjusted by comparing simulated and measured moisture results. The vapor resistance in radial and tangential directions has a negligible influence on results. Vapor resistance factors in these two directions are obtained from Zillig [39]. Fig. 6b shows the vapor resistance factor in the different directions of spruce wood. The relation between vapor permeability and vapor resistance factor is:

$$\delta_v = \frac{\delta_a}{\mu} \tag{15}$$

where $\delta_a$ is the vapor permeability in dry air, which is given by the Schirmer's equation [40].

### 4.3. Thermal properties

Sonderegger et al. [41] measured thermal conductivity at different moisture content in spruce wood. An increase in moisture content shows a small increase in thermal conductivity. Kühlmann [42] measured the linear relation between the bulk density of wood and thermal conductivity. The thermal conductivity of the sample here is calculated based on results from Sonderegger et al. [41] with the bulk density of the spruce sample as the scaling factor. The thermal conductivity is calculated as follows:

$$\lambda(w) = \frac{\rho}{\rho_{so}} \lambda_{so}(w) \tag{16}$$

where $\rho$ is the dry bulk density of our spruce wood sample, $\rho_{so}$ is the dry bulk density of spruce wood sample from Sonderegger et al. [41], and $\lambda_{so}(w)$ is the thermal conductivity of spruce wood sample at different moisture content obtained from Sonderegger et al. [41].

Fig. 6c shows the relation between thermal conductivity and moisture content for the different directions in spruce wood at the density of the samples used in our experiments.

### 4.4. Initial and boundary conditions

For the adsorption experiment, the conditioning period has almost negligible influence. Therefore, the simulation starts from the beginning of the experimental period. By comparison, the conditioning period has some influence on moisture and heat transport in the desorption sample. Therefore, the simulation starts from the beginning of the conditioning period. The initial conditions for the adsorption sample are a uniform relative humidity of 5.5% RH and a temperature of 30 °C and for the desorption sample a relative humidity of 90.5% RH and a temperature of 28.2 °C. The boundary temperature and relative humidity conditions for the adsorption and desorption experiments are illustrated in Fig. 2.

The wood samples are insulated laterally with XPS. The lateral heat flux is calculated as follows:

$$Q_L = \frac{\lambda_{XPS}}{d}(T_{amb} - T) \tag{17}$$

where $T_{amb}$ is the ambient temperature (°C), $T$ is the temperature on the wood sample surface (°C), $\lambda_{ins}$ is the thermal conductivity of the XPS (W/mK), $d$ is the thickness of the XPS layer (m).

The lateral vapor flux is calculated as follows:

$$g_L = \frac{\delta_{XPS}}{d}\left(p_{v,amb} - p_v\right) \tag{18}$$

where $p_{v,amb}$ is the vapor pressure in the ambient environment (Pa), $p_v$ is the vapor pressure on the surface of the wood sample (Pa), $\delta_{XPS}$ is the vapor permeability of XPS (s), $d$ is the thickness of the XPS layer (m). The thickness of the XPS layer is 1.0 cm and the thermal conductivity and vapor permeability of XPS is 0.3 W/m/k and $2.0 \times 10^{-12}$ s, respectively. Considering the much smaller area and much larger thickness of the insulation layer at the front, back and bottom surfaces, the heat and vapor fluxes at these locations are neglected and non-flux conditions are imposed on these surfaces.

The heat flux at the top surface is described with convective heat flux and sensible and latent heat flux due to vapour transfer. The heat flux ($Q_T$) is calculated based on the following equation:

$$Q_T = h_T(T_{air} - T) + \left(c_v\left(T - T_{ref}\right) + L_m\right)g_T \tag{19}$$

where $h_T$ is the convective heat transfer coefficient (W/m$^2$K), $T_{air}$ is the incoming air temperature (K), $T$ is the wood surface temperature (K). The convective heat transfer coefficient is chosen based on CFD simulation of the airflow in the custom-made micro-wind tunnel and then slightly adjusted by comparing simulated and measured temperature results. The determined convective heat transfer coefficient is 20.0 W/m$^2$K. $g_T$ is the vapor flux at the top surface (kg/m$^2$s).

The vapor flux at the top surface is calculated as:

$$g_T = h_v\left(p_{v,air} - p_v\right) \tag{20}$$

where $h_v$ is the vapor transfer coefficient (s/m), $T_e$ is the incoming air temperature (K), $p_{v,air}$ is the vapor pressure of the incoming air (Pa), $p_v$ is the vapor pressure at the wood surface (Pa). The vapor transfer coefficient ($h_v$) is obtained from the convective heat transfer coefficient using the Lewis analogy: $h_v = h_T \times 7.7 \times 10^{-9}$.

The enthalpy of sorbed water is smaller than the enthalpy of liquid water and water vapor. When the adsorbed water in the wood evaporates to vapor, the associated latent heat is the sum of latent heat of vaporization of water and the differential heat of sorption. The differential heat of sorption $\Delta H_s$ in wood can be calculated based on two isotherms at different temperatures using the Clausius-Clapeyron equation:

$$\Delta H_s = R_v \frac{\ln RH_2 - \ln RH_1}{\frac{1}{T_1} - \frac{1}{T_2}} \tag{21}$$

where RH is the relative humidity, T is the temperature (K), $R_v$ is the gas constant of water (kJ/kg k). The adsorption and desorption isotherms at 20 °C and 40 °C are used for the calculation of the differential heat of sorption (Fig. 7). The difference of adsorption isotherms at 20 °C and 40 °C is smaller than that for the desorption isotherms, which leads to smaller heat of sorption in adsorption. $\Delta H_s$ is then added to the latent heat of vaporization ($2.44 \times 10^6$ [J/kg]) to yield the latent of moisture of wood as described by equation (9) above.

## 5. Results

Figs. 8 and 9 compare simulated and measured moisture content and temperature variations in the adsorption experiment and Figs. 10 and 11 for the desorption experiment. Overall, the simulated moisture content and temperature variations agree with the experimental ones. In general, the agreement between measurement and simulation is better for the adsorption experiment than the desorption one. The discrepancy between simulation and measurement could be caused by the uncertainty of material properties. Wood is a heterogeneous material and the adsorption and desorption samples could show different material properties. Here the same hygrothermal properties are used for both samples. The vapor permeability is only related to RH and thus the same for both adsorption and desorption processes, although differences may exist between vapor permeability in ad- and desorption. In our simulations, different sorption curves and differential heat of sorption are used for ad- and desorption. In addition, the thermal conductivity of the samples is obtained from literature, and some uncertainty may exist on the thermal conductivity.

The large temperature change at the beginning of both experiments is reproduced well by the numerical model. The low vapor resistance factor in the longitudinal direction leads to a fast vapor transport in the samples. The large temperature change at the beginning of the adsorption and desorption experiment is due to the large adsorption and desorption rate. Fig. 12 shows the moisture content variation rate during the adsorption and desorption experiments. A large moisture change rate is associated with a large release and absorption of latent heat. The moisture content variation rate is highest at the beginning of the experiment and decreases with time. When the moisture variation rate slows down, the effect of latent heat on temperature decreases. Consequently, more heat can flow from/to the boundary and the temperature presents less change.

We proceed with a parametric study on the influence of thermal conductivity, vapor resistance factor and convective heat transfer coefficient on the sorption process. The influence of different parameters on

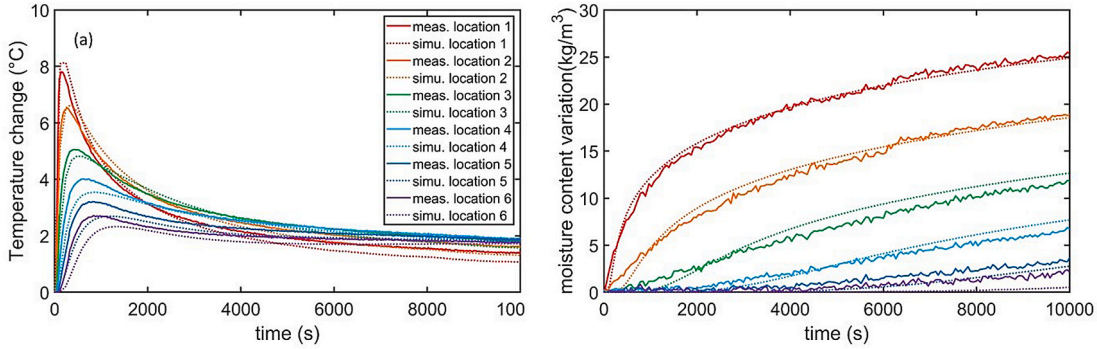


**Fig. 8.** (a) Comparison of measured and simulated (a) temperature and (b) moisture content variation in the adsorption experiment.

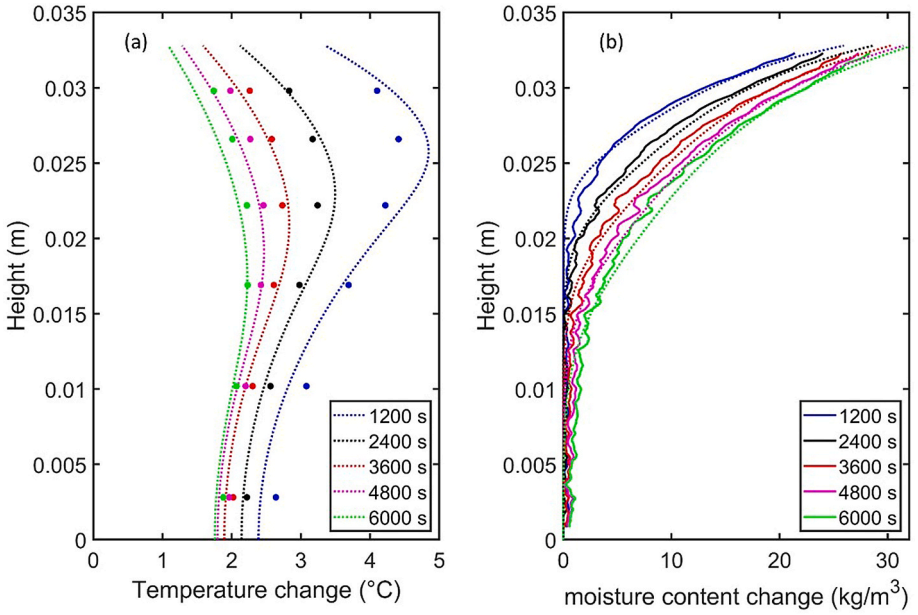


**Fig. 9.** Comparison of the measured and simulated (a) temperature and (b) moisture content profiles in the adsorption experiment (the dot and the solid line represent measured results and the dashed line represents the simulated ones).

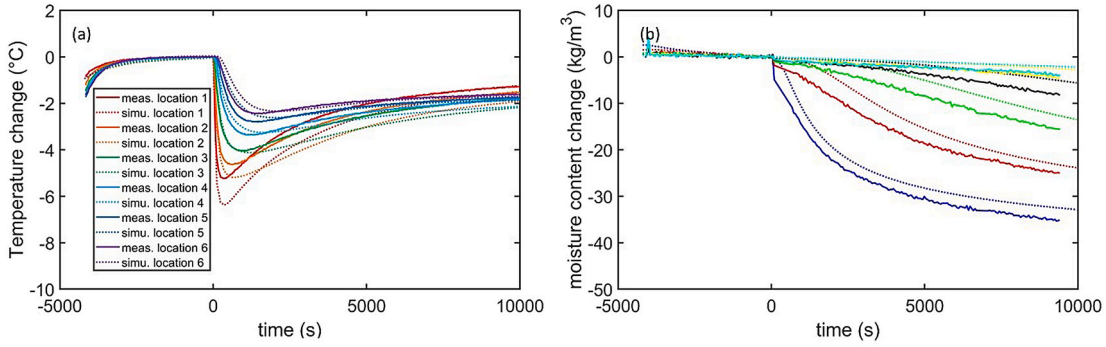


**Fig. 10.** Comparison of the measured and simulated (a) temperature and (b) moisture content variation in the desorption experiment.

temperature and moisture content variation is analyzed. We evaluate the influence of the parameters by changing their values by −50%, −25%, 0%, 25% and 50%. Fig. 13a shows the influence of thermal conductivity on moisture content and temperature change. The thermal conductivity has almost no influence on moisture content change. By comparison, the influence of thermal conductivity on temperature change is significant. An increase in thermal conductivity leads to faster heat transport and in turn to smaller variations in temperature profiles.

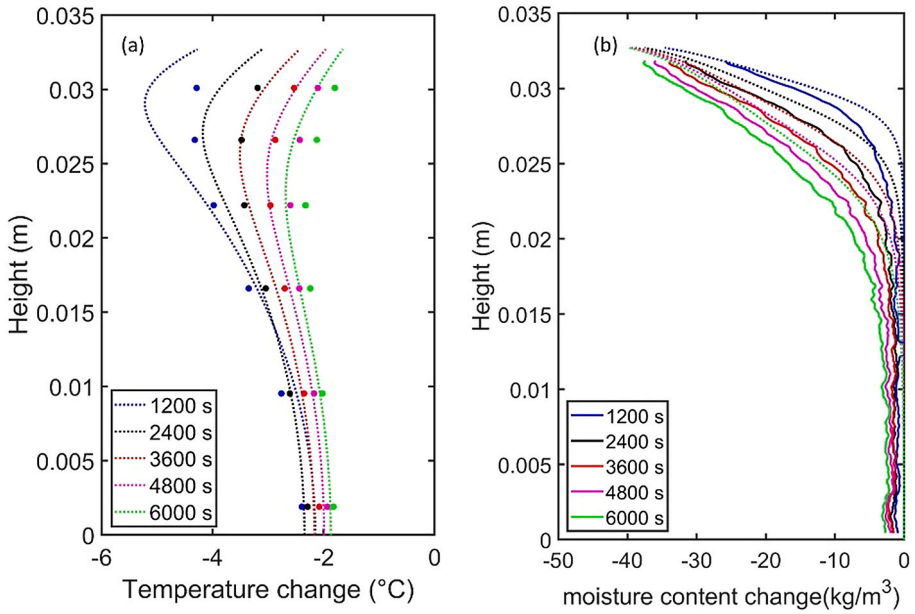


**Fig. 11.** Comparison of the measured and simulated (a) temperature and (b) moisture content profiles in the desorption experiment (the dot and the solid line represent measured results and the dashed line represents the simulated ones).

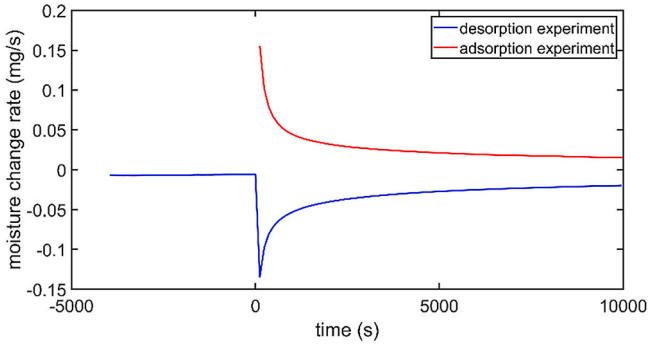


**Fig. 12.** Simulated total moisture change rate in the sample during adsorption and desorption experiment.

By contrast, the vapor resistance factor has a large influence on both moisture content and temperature change (Fig. 13b). An increase in vapor resistance factor leads to slower vapor transport and thus to smaller moisture content increase. Meanwhile, a smaller moisture content increase involves less latent heat released during adsorption. As a result, the temperature increase is lower due to an increase in the vapor resistance factor. According to the Lewis analogy, a change in convective heat transfer coefficient results in also a change in vapor transfer coefficient. However, the change in convective heat transfer coefficient and thus the change in vapor transfer coefficient have a very small influence on moisture content change (Fig. 13c). The limiting factor for vapor transport in the sample is the vapor permeability of the sample. As a result, a change in surface vapor transfer coefficient has a small influence on moisture transport in the sample. By comparison, the change in convective heat transfer coefficient has a large influence on heat transport. An increase in convective heat transfer coefficient leads to a decrease in temperature in the sample. It is because an increase in convective heat transfer coefficient will increase the influence of the boundary condition on heat transport in the sample, which results in smaller temperature change caused by sorption processes. Therefore, vapor resistance factor has an influence on both moisture and heat transport while thermal conductivity and convective heat transfer coefficient have an influence only on heat transport. The vapor transfer coefficient has a small influence on vapor transport because vapor transport is limited by vapor diffusion resistance of the sample. As vapor resistance factor, thermal conductivity and convective heat transfer coefficient all have an influence on heat transport, an uncertainty in one parameter will result in uncertainty in other parameters.

## 6. Discussion on test setups to determine moisture buffering value (MBV)

Sorption of vapor during the moisture buffering tests is accompanied by temperature variations in the samples. So far, moisture buffering tests have disregarded co-occurring thermal phenomena. The magnitude of temperature variation within a sample depends on the presence or not of thermal insulation around the sample. Actually, heat flows at the sample borders may affect vapor transport and different thermal conditions may lead to differences in MBV.

Here we study the influence of the presence of an insulation layer on the MBV of a sample of spruce in the longitudinal direction. The validated hygrothermal model is used for this numerical analysis where the test protocol of NORDTEST is followed as the base case and a second case considers the sample to be insulated. All simulations are performed three-dimensionally, and the length and width of the samples are 10.0 cm, while the thickness of the sample ranges from 0.2 to 3.0 cm. All the surfaces but the top one are assumed to be totally sealed for vapor transport. The initial relative humidity and temperature of the samples are 75% and 23.0 °C, respectively. The ambient air is controlled at 23.0 °C. The samples are exposed to 16 h of a RH of 33% followed by 8 h of a RH of 75%. The humidity cycle is repeated 10 times to ensure that daily variations of moisture adsorption and desorption are stable at the last cycle. The vapor transfer coefficient is first chosen to be the same as required in the NORDTEST: $4.8 \times 10^7$ $m^2/s$ Pa/kg. The convective heat transfer coefficient is derived based on the Lewis analogy, which is 2.6 $W/m^2/K$. To consider the influence of surface transfer coefficient on MBV, simulations are also performed for cases where both vapor transfer coefficient and convective heat transfer coefficient are increased by 50% and 100%. For the thermally insulated sample, all the surfaces but the

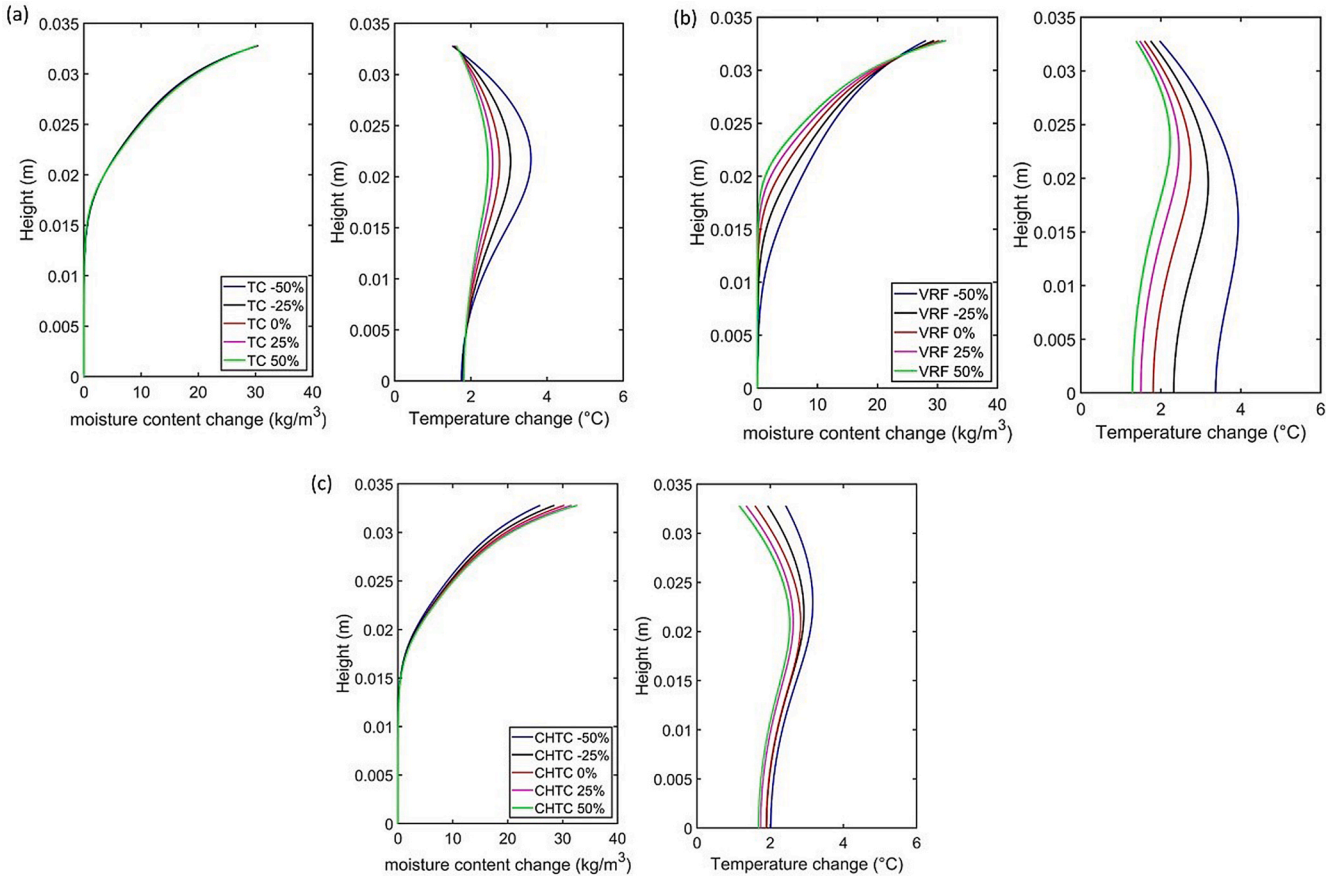


**Fig. 13.** (a) Influence of thermal conductivity (TC) on moisture content and temperature variation profiles at t = 3600s during adsorption; (b) Influence of vapor resistance factor (VRF) on moisture content and temperature variation profiles at t = 3600s during adsorption; (c) Influence of convective heat transfer coefficient (CHTC) on moisture content and temperature variation profiles at t = 3600s during adsorption.

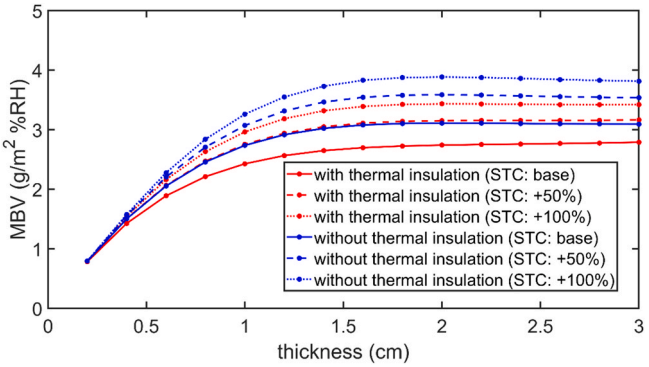


**Fig. 14.** MBV for wood sample of varying thicknesses for samples with thermal insulation (unidirectional) and without thermal insulation (omnidirectional). (STC: surface transfer coefficient).

exposed one are insulated with 5.0 cm of XPS insulation material. Fig. 14 shows the comparison of MBV for different sample thicknesses for the samples with and without thermal insulation under the different surface transfer coefficients. When the thickness of the sample is 0.2 cm, the MBV is almost the same for the scenarios with and without thermal insulation. This is due to the small thickness of the sample. Under this condition, heat transport is dominated by the direction normal to the exposed direction and lateral heat transport has negligible influence. For such a thin sample, the influence of lateral heat transport is limited. The difference of MBV between the two scenarios increases with an increase in thickness of the sample. For example, the difference in MBV between the two scenarios reaches 0.38 g/m$^2$ %RH for a thickness of 1.8 cm and the base surface transfer coefficient, corresponding to a difference of 14.0% between the two MBVs. A further increase in the sample thickness does not lead to much change in the difference in MBV. Fig. 14 shows also clearly that an increase in surface transfer coefficient leads to an increase in MBV. The increase in MBV is smaller for larger surface transfer coefficient. For example, for the sample with a thickness of 1.8 cm and thermal insulation, the MBV increases by 0.41 g/m$^2$ %RH from the base case to the STC +50% case. By comparison, the increase is 0.28 g/m$^2$ %RH from the STC +50% case to the STC +100% case. When the thickness of the sample is very small, e.g. smaller than 0.4 cm, the influence of surface transfer coefficient is almost negligible. That is because vapor and heat transport in very thin samples are not limited by surface transfer coefficient.

The difference in MBV in the samples with and without insulation is caused by the temperature difference. Although the ambient temperature is constant at 23.0 °C, there is still a considerable change of temperature in the samples during adsorption and desorption. For example, for the sample with a thickness of 1.8 cm and thermal insulation, the temperature increases to 26.6 °C during adsorption and decreases to 20.5 °C during desorption (Fig. 15a). By comparison, when the sample is not thermally insulated, the temperature change is smaller. The temperature change for the sample without thermal insulation could be up to 1.0 °C smaller than the scenario with thermal insulation. The difference in temperature change leads also to a difference in moisture content change in the sample. In non-isothermal condition, vapor transfer can also be caused by thermal gradients. During the desorption period, temperature at the shallower depth is larger than at the greater depth (Fig. 15b). Consequently, there is vapor flux from air to the sample and

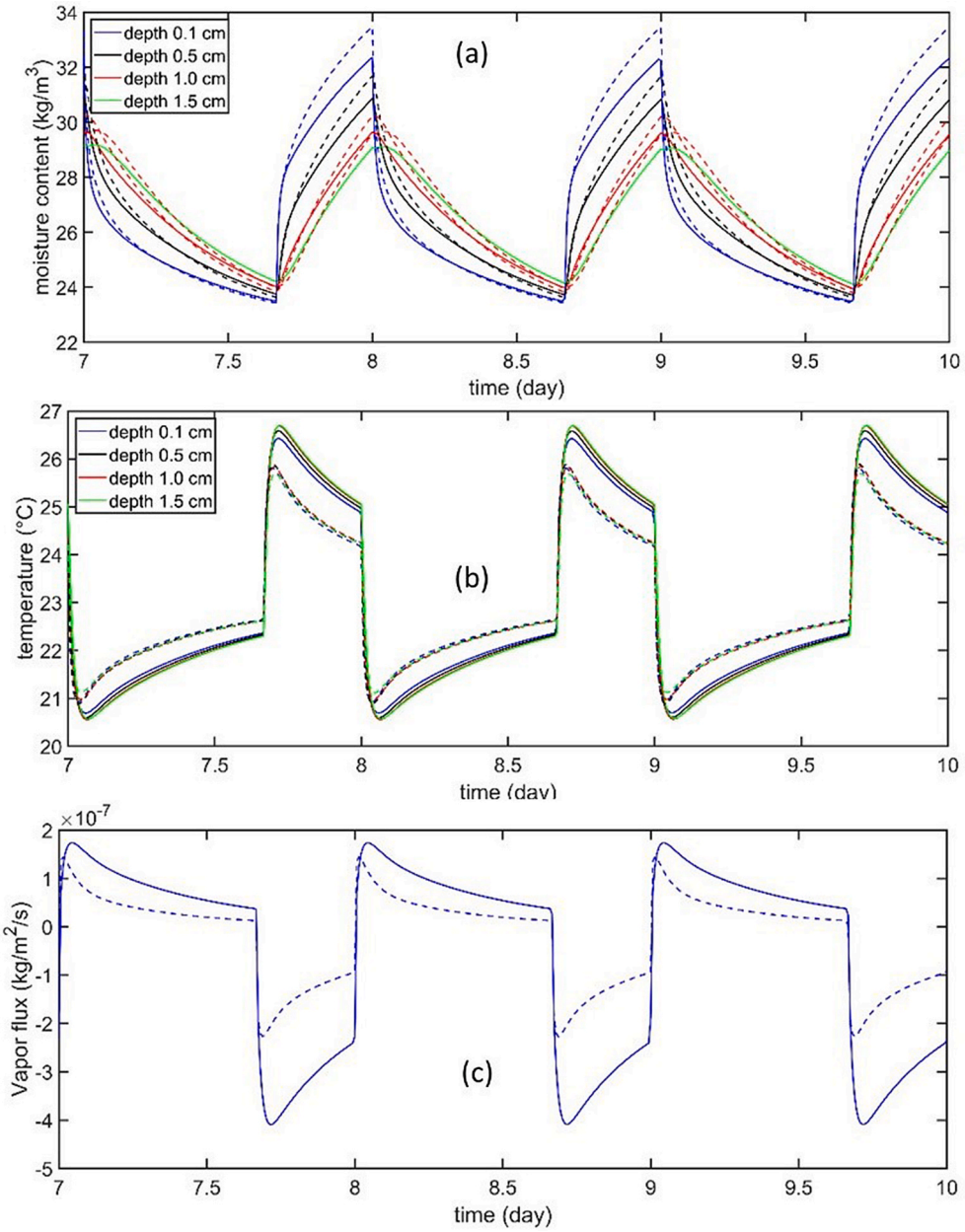


**Fig. 15.** (a) Moisture content at three depths for the scenarios with sample thickness of 1.8 cm; (b) temperature at three depths for the scenarios with sample thickness of 1.8 cm; (c) vapor flux at the top surface due to temperature gradient (positive value: vapor flux flowing to the sample; negative value: vapor flux leaving the sample). The solid line represent the sample with insulation and the dashed line represent the scenario without insulation.

thus leads to moisture gain in the sample. By contrast, during the adsorption period, temperature at the shallower depth is smaller than at the greater depth. Consequently, there is vapor flux from the sample to the air and thus leads to moisture loss in the sample. In general, there is more moisture loss caused by temperature induced vapor flow for the sample with insulation than for the sample without insulation (Fig. 15c). Consequently, the sample without insulation shows larger moisture content variations. Therefore, the sample without thermal insulation presents a larger moisture content change (Fig. 15a), which consequently leads to a larger MBV.

In general, it is recommended to thermally insulate, in addition to the vapor sealing, the samples for MBV tests. For building materials with low hygroscopicity, the difference of MBV between samples with and without insulation layer may be small. However, for very hygroscopic materials, there will be a very large change of temperature during adsorption and desorption. Some new types of composite materials such as Metal-Organic Frameworks (MOFs) are very hygroscopic and can show a MBV up to 15.0 g/m$^2$ %RH [43,44]. For these materials, the difference of MBV between the sample with thermal insulation and without thermal insulation may be very large. It is necessary to insulate highly hygroscopic materials in the MBV tests as insulated conditions are closer to actual conditions, where the surface finishing materials are not only exposed to unidirectional vapor transport but also unidirectional heat transport.

## 7. Conclusions

Vapor adsorption and desorption experiments are performed to study the coupled vapor and heat transport in spruce samples along the longitudinal direction. Neutron radiography and wireless thermocouples are used to measure moisture content and temperature changes during the experiments, respectively. A hygrothermal model is presented to

simulate vapor and heat transport during adsorption and desorption experiments. In general, there is very good agreement between measured and simulated moisture content and temperature changes. Moisture adsorption and desorption lead to a significant change in temperature in both adsorption and desorption experiments. It is observed that the vapor resistance factor has an influence on both vapor and heat transport while thermal conductivity has only an influence on heat transport. The vapor transfer coefficient has a small influence on vapor transport because vapor transport is limited by vapor diffusion resistance of the sample. By comparison, the convective heat transfer coefficient has an influence on heat transport. The validated hygrothermal model is used to study the influence of the presence of an insulation layer around the samples in a moisture buffering test (MBV). The latent heat associated with moisture adsorption and desorption leads to non-isothermal conditions in samples for moisture buffering tests although the ambient temperature is kept constant. The insulation may considerably affect the temperature in the samples and thus MBV in moisture buffering tests. The difference of MBV with and without insulation layer for spruce in the longitudinal direction may reach 14%. For more hygroscopic materials, the difference may be even much larger. It is recommended to not only seal and but also insulate the samples for MBV tests, as the finishing building materials in building surfaces are normally exposed to both unidirectional vapor and heat transport.

## CRediT authorship contribution statement

**Xiaohai Zhou:** Writing – review & editing, Writing – original draft, Visualization, Methodology, Investigation, Conceptualization. **Guylaine Desmarais:** Conceptualization, Investigation, Writing – original draft. **Stephan Carl:** Resources. **David Mannes:** Investigation. **Dominique Derome:** Funding acquisition, Supervision, Writing – review & editing. **Jan Carmeliet:** Writing – review & editing, Supervision, Funding acquisition.

## Declaration of competing interest

The authors declare that they have no known competing financial interests or personal relationships that could have appeared to influence the work reported in this paper.

## Acknowledgments

The authors would like to acknowledge the contribution and support of Bruno Binder, Roger Vonbank and Beat Margelisch at Empa, of Jan Hovind and Peter Vontobel at the Paul Scherrer Institute (PSI), as well as of doctoral student at ETH Zurich Marcelo Parada, for their help with the project.

## References

[1] C.J. Simonson, M. Salonvaara, T. Ojanen, Moderating indoor conditions with hygroscopic building materials and outdoor ventilation, Build. Eng. 110 (2004).
[2] H. Derluyn, H. Janssen, J. Diepens, D. Derome, J. Carmeliet, Hygroscopic behavior of paper and books, J. Build. Phys. 31 (2007) 9–34.
[3] H. Ge, X. Yang, P. Fazio, J. Rao, Influence of moisture load profiles on moisture buffering potential and moisture residuals of three groups of hygroscopic materials, Build. Environ. 81 (2014) 162–171.
[4] F. Collet, S. Pretot, Experimental investigation of moisture buffering capacity of sprayed hemp concrete, Construct. Build. Mater. 36 (2012) 58–65.
[5] O.F. Osanyintola, C.J. Simonson, Moisture buffering capacity of hygroscopic building materials: experimental facilities and energy impact, Energy Build. 38 (2006) 1270–1282.
[6] M. Woloszyn, T. Kalamees, M.O. Abadie, M. Steeman, A.S. Kalagasidis, The effect of combining a relative-humidity-sensitive ventilation system with the moisture-buffering capacity of materials on indoor climate and energy efficiency of buildings, Build. Environ. 44 (2009) 515–524.
[7] S. Hameury, Moisture buffering capacity of heavy timber structures directly exposed to an indoor climate: a numerical study, Build. Environ. 40 (2005) 1400–1412.
[8] M. Zhang, M. Qin, C. Rode, Z. Chen, Moisture buffering phenomenon and its impact on building energy consumption, Appl. Therm. Eng. 124 (2017) 337–345.
[9] X. Zhou, J. Carmeliet, M. Sulzer, D. Derome, Energy-efficient mitigation measures for improving indoor thermal comfort during heat waves, Appl. Energy 278 (2020) 115620.
[10] D. Kraniotis, N. Langouet, T. Orskaug, K. Nore, G. Glasø, Moisture buffering and latent heat sorption phenomena of a wood-based insulating sandwich panel, in: Proceedings of World Conference on Timber Engineering, 2016, pp. 22–26.
[11] S. Charisi, D. Kraniotis, K. Nore, Latent heat sorption phenomena in three building materials: Norwegian spruce (picea abies), gypsum board and concrete, in: Proceedings of World Conference on Timber Engineering, 2016.
[12] N. Holcroft, A. Shea, Moisture buffering and latent heat effects in natural fibre insulation materials, Port. SB13-Contribution Sustain. Build. to Meet EU (2013) 221–228.
[13] T. Zhao, E. Ma, W. Zhang, Moisture and temperature changes of wood during adsorption and desorption processes, Wood Fiber Sci. 45 (2013) 187–194.
[14] C. James, C.J. Simonson, P. Talukdar, S. Roels, Numerical and experimental data set for benchmarking hygroscopic buffering models, Int. J. Heat Mass Tran. 53 (2010) 3638–3654.
[15] D. Lelievre, T. Colinart, P. Glouannec, Hygrothermal behavior of bio-based building materials including hysteresis effects: experimental and numerical analyses, Energy Build. 84 (2014) 617–627.
[16] H.M. Künzel, Simultaneous Heat and Moisture Transport in Building Components, One-And Two-Dimensional Calc. Using Simple Parameters, IRB-Verlag Stuttgart, 1995.
[17] J. Grunewald, Diffusiver und konvektiver Stoff-und Energietransport in kapillarporösen Baustoffen, Diss. TU Dresden, Dresden, Germany, 1997.
[18] H. Janssen, B. Blocken, J. Carmeliet, Conservative modelling of the moisture and heat transfer in building components under atmospheric excitation, Int. J. Heat Mass Tran. 50 (2007) 1128–1140.
[19] X. Zhou, D. Derome, J. Carmeliet, Hygrothermal modeling and evaluation of freeze-thaw damage risk of masonry walls retrofitted with internal insulation, Build. Environ. 125 (2017) 285–298.
[20] M. Koniorczyk, D. Gawin, Heat and moisture transport in porous building materials containing salt, J. Build. Phys. 31 (2008) 279–300.
[21] X. Zhou, J. Carmeliet, D. Derome, Assessment of moisture risk of wooden beam embedded in internally insulated masonry walls with 2D and 3D models, Build. Environ. (2020) 107460.
[22] X. Zhou, J. Carmeliet, D. Derome, Influence of envelope properties on interior insulation solutions for masonry walls, Build. Environ. 135 (2018) 246–256, https://doi.org/10.1016/j.buildenv.2018.02.047.
[23] E. Vereecken, S. Roels, Capillary active interior insulation: do the advantages really offset potential disadvantages? Mater. Struct. 48 (2015) 3009–3021.
[24] H.M. Künzel, Effect of interior and exterior insulation on the hygrothermal behaviour of exposed walls, Mater. Struct. 31 (1998) 99–103.
[25] D. Gawin, F. Pesavento, M. Koniorczyk, B.A. Schrefler, Non-equilibrium modeling hysteresis of water freezing: ice thawing in partially saturated porous building materials, J. Build. Phys. 43 (2019) 61–98.
[26] H. Derluyn, P. Moonen, J. Carmeliet, Deformation and damage due to drying-induced salt crystallization in porous limestone, J. Mech. Phys. Solid. 63 (2014) 242–255.
[27] M. Qin, R. Belarbi, A. Aït-Mokhtar, F. Allard, Simulation of coupled heat and moisture transfer in air-conditioned buildings, Autom. ConStruct. 18 (2009) 624–631.
[28] T. Colinart, D. Lelièvre, P. Glouannec, Experimental and numerical analysis of the transient hygrothermal behavior of multilayered hemp concrete wall, Energy Build. 112 (2016) 1–11.
[29] H.-J. Steeman, M. Van Belleghem, A. Janssens, M. De Paepe, Coupled simulation of heat and moisture transport in air and porous materials for the assessment of moisture related damage, Build. Environ. 44 (2009) 2176–2184.
[30] C. Rode, R. Peuhkuri, B. Time, K. Svennberg, T. Ojanen, Moisture buffer value of building materials, J. ASTM Int. (JAI) 4 (2007) 1–12.
[31] J.S. Association, Test method of adsorption/desorption efficiency for building materials to regulate an indoor humidity–Part 1: response method of humidity, JIS A (2002) 1470e1, 2002.
[32] X. Zhou, G. Desmarais, P. Vontobel, J. Carmeliet, D. Derome, Masonry brick–cement mortar interface resistance to water transport determined with neutron radiography and numerical modeling, J. Build. Phys. 44 (3) (2020) 251–271.
[33] R. Hassanein, H.O. Meyer, A. Carminati, M. Estermann, E. Lehmann, P. Vontobel, Investigation of water imbibition in porous stone by thermal neutron radiography, J. Phys. D Appl. Phys. 39 (2006) 4284–4291.
[34] S. Lal, L.D. Poulikakos, M. Sedighi Gilani, I. Jerjen, P. Vontobel, M.N. Partl, J. C. Carmeliet, D. Derome, Investigation of water uptake in porous asphalt concrete using neutron radiography, Transport Porous Media 105 (2014) 431–450.
[35] C.-E. Hagentoft, A.S. Kalagasidis, B. Adl-Zarrabi, S. Roels, J. Carmeliet, H. Hens, J. Grunewald, M. Funk, R. Becker, D. Shamir, Assessment method of numerical prediction models for combined heat, air and moisture transfer in building components: benchmarks for one-dimensional cases, J. Therm. Envelope Build. Sci. 27 (2004) 327–352.
[36] E.A. Guggenheim, Applications of Statistical Mechanics, Clarendon Press, 1966.
[37] R.B. Anderson, W.K. Hall, Modifications of the brunauer, emmett and teller equation II1, J. Am. Chem. Soc. 70 (1948) 1727–1734.
[38] E.O. Timmermann, Multilayer sorption parameters: BET or GAB values? Colloids Surfaces A Physicochem. Eng. Asp. 220 (2003) 235–260.

[39] W. Zillig, Moisture Transport in Wood Using a Multiscale Approach, Diss. Kathol. Univ. Leuven, Leuven, Belgium, 2009.
[40] R. Schirmer, Die Diffusionszahl von Wasserdampf-Luft-Gemischen und die Verdampfungsgeschwindigkeit, VDI-Verlag, 1938.
[41] W. Sonderegger, S. Hering, P. Niemz, Thermal behaviour of Norway spruce and European beech in and between the principal anatomical directions, Holzforschung 65 (2011) 369–375.
[42] G. Kühlmann, Untersuchung der thermischen Eigenschaften von Holz und Spanplatten in Abhängigkeit von Feuchtigkeit und Temperatur im hygroskopischen Bereich, Holz Als Roh-Und Werkst 20 (1962) 259–270.
[43] K. Zu, M. Qin, C. Rode, M. Libralato, Development of a moisture buffer value model (MBM) for indoor moisture prediction, Appl. Therm. Eng. 171 (2020) 115096.
[44] S. Cui, M. Qin, A. Marandi, V. Steggles, S. Wang, X. Feng, F. Nouar, C. Serre, Metal-Organic Frameworks as advanced moisture sorbents for energy-efficient high temperature cooling, Sci. Rep. 8 (2018) 1–9.